JACS
JOURNAL OF THE AMERICAN CHEMICAL SOCIETY
Communication
pubs.acs.org/JACS

Self-Focusing by Ostwald Ripening: A Strategy for Layer-by-Layer Epitaxial Growth on Upconverting Nanocrystals

Noah J. J. Johnson,[†] Andreas Korinek,[‡] Cunhai Dong,[†] and Frank C. J. M. van Veggel*[,†]

[†]Department of Chemistry, University of Victoria, Victoria, BC V8W 3V6, Canada
[‡]Canadian Centre for Electron Microscopy, McMaster University, Hamilton, ON L8S 4L7, Canada

Supporting Information

ABSTRACT: We demonstrate a novel epitaxial layer-by-layer growth on upconverting $NaYF_4$ nanocrystals (NCs) utilizing Ostwald ripening dynamics tunable both in thickness and composition. Injection of small sacrificial NCs (SNCs) as shell precursors into larger core NCs results in the rapid dissolution of the SNCs and their deposition onto the larger core NCs to yield core−shell structured NCs. Exploiting this NC size dependent dissolution/growth, the shell thickness can be controlled either by manipulating the number of SNCs injected or by successive injection of SNCs. In either of these approaches, the NCs self-focus from an initial bimodal distribution to a unimodal distribution (σ <5%) of core−shell NCs. The successive injection approach facilitates layer-by-layer epitaxial growth without the need for tedious multiple reactions for generating tunable shell thickness, and does not require any control over the injection rate of the SNCs, as is the case for shell growth by precursor injection.

Epitaxial shell growth on colloidal nanocrystals (NCs) is a widely employed strategy to separate spatially the optically active core from the surrounding environment, or to generate NCs with multifunctionality. In case of lanthanide-based upconverting NCs, shell growth is an attractive option for enhancing the inherently low quantum efficiency of the upconversion (UC) process.[1] The unique UC process, which converts multiple low-energy photons to a high-energy photon facilitated by the Ln^{3+} dopants in $NaLnF_4$ NCs, is attractive for a wide range of applications.[2] These multiphoton absorption and relaxation processes are easily quenched by the high-energy vibrations of solvent molecules, and epitaxial shell growth has been shown to enhance the efficiency of the UC process.[1b] While in principle thick shells are ideal for enhanced UC efficiency, integrating the UC process for other applications such as luminescence resonance energy transfer (LRET), energy migration-mediated upconversion (EMU), metal enhanced luminescence, photoswitches, and optically driven actuators requires modulation of the thickness of the epitaxial layers to facilitate efficient energy transfer/enhancement.[3] As these applications are highly dependent on the spatial separation of the organic molecules/metal centers/dopant ions from the UC core, a highly tunable layer-by-layer epitaxial growth becomes particularly important.

While there has been promising progress in epitaxial growth, fundamental limitations and challenges in generating easily tunable shell growth are not fully addressed. The growth mechanism of $NaLnF_4$ (Ln: Pr to Lu, Y) NCs is known to vary along the series; while the light lanthanides favor hexagonal phase (β), the cubic phase (α) is preferred in heavy lanthanides. Liu et al. used this fundamental property to control simultaneously the size and phase of $NaYF_4$ NCs.[4] We have observed that this preference of crystal phase also affects the epitaxial shell growth process. In the widely used seed-mediated shell growth on β-$NaYF_4$, the shell precursors preferentially nucleate as α-$NaYF_4$ and a ripening-mediated process leads to core−shell NCs (Figure S1), contrary to generally assumed mechanism of the core NCs acting as nuclei/seeds for subsequent growth.[1f] This deviation from the conventional growth mode greatly restricts the ability to tune the layer thickness as multiple parameters need to be controlled precisely and simultaneously. The fact that the rate of active monomer formation will vary with the molecular precursor concentration which is directly related to time and temperature makes it cumbersome to tune shell growth as recently reported,[3d] as this relies on a trial-and-error approach. To overcome these limitations, we have developed a novel approach of self-focusing by Ostwald ripening for achieving layer-by-layer growth directly onto a core NC. This method eliminates the need for precise control of multiple parameters/reactions to obtain tunable shell growth.

In colloidal systems, larger particles with smaller surface to volume ratios are favored over the energetically less stable smaller particles, resulting in the growth of larger particles at the expense of smaller ones, referred to as Ostwald ripening. Ripening typically leads to size broadening, and one usually aims to avoid ripening so as to obtain NCs with a narrow size distribution. However, theoretical studies on ripening in an ensemble of differently sized NCs have shown that the ensemble size focuses unlike the asymmetric broadening predicted by LSW (Lifshitz−Slyozov−Wagner) theory.[5] While it has been more than a decade since these theoretical studies, reports on ripening-mediated self-focusing have been limited to observations of such a pathway during growth of various semiconductor/inorganic NCs.[6] To date, no reports on the deliberate use of this unique self-focusing process as a synthetic tool to tune the structure/property of NCs has been realized. In this context, we conceptualized that injection of

Received: March 20, 2012
Published: June 26, 2012

ACS Publications © 2012 American Chemical Society

dx.doi.org/10.1021/ja302717u | J. Am. Chem. Soc. 2012, 134, 11068−11071

small sacrificial NCs (SNCs) into a solution of core NCs (defocusing) should ideally lead to the dissolution of SNCs and deposition on the larger core NCs (self-focusing) resulting in epitaxial growth of the larger NCs. Repeating the defocusing and self-focusing cycle should allow for layer-by-layer growth, without the need for any stringent requirements in generating tunable epitaxial layer growth.

Undoped α-$NaYF_4$ NCs (~6.5 nm) were synthesized and used as SNCs.[7] Using lanthanide ions in appropriate molar ratio, upconverting β-$NaYF_4$:Yb^{3+}, Er^{3+} NCs were synthesized at 300 °C for 1 h.[8] After 1 h at 300 °C when core NCs had formed, calculated amounts of SNCs (0.65 mmol) in 1-octadecene (1 mL) were injected and allowed to ripen (10 min) before cooling the mixture to room temperature. Aliquots of reaction mixture: core NCs (t = 0), right after SNC injection (t = 5 s), and the final product (t = 10 min) were retrieved, washed, and dispersed in hexane for analysis by transmission electron microscopy (TEM) and X-ray diffraction (XRD) shown in Figure 1 and Figure S3.

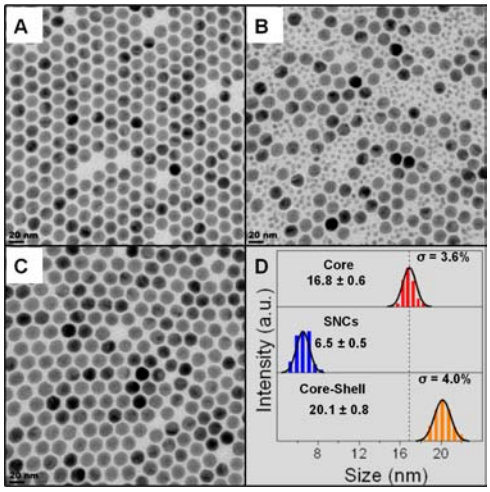

Figure 1. (A–C) TEM of $NaYF_4$:Yb^{3+}/Er^{3+} (15/2%) core NCs (t = 0), after injection of sacrificial α-$NaYF_4$ NCs (t = 15 s), and after self-focusing $NaYF_4$:Yb^{3+}/Er^{3+} (15/2%) core/$NaYF_4$ shell NCs (t = 10 min), respectively, and (D) size distribution of the NCs.

The TEM analysis (Figure 1A–C and Figure S3) of the three aliquots confirms the complete dissolution and deposition of the SNCs on core NCs. The core NCs 16.8 ± 0.6 nm has grown into a unimodal size distribution of larger 20.1 ± 0.8 nm NCs after 10 min ripening. The aliquot retrieved right after SNC injection shows a bimodal distribution (Figure 1B), corresponding to the presence of core NCs and injected SNCs. Importantly, the size increase strictly correlates to the amount of SNCs injected, accounting for the mass balance during the dissolution/growth process. The XRD patterns indicate (Figure S3) that the core NCs are of hexagonal phase, and after SNC (cubic NCs) injection in the bimodal size regime, a small peak arising from the 111 plane of cubic SNCs (42°2θ), completely vanished after ripening to yield hexagonal phase NCs. During ripening, the cubic SNCs dissolve and deposit as hexagonal layers on the core NCs; the monomers/adatoms released from the SNCs adapt to the NC surface onto which they deposit. The epitaxial layer thickness can readily be tuned by simply manipulating the amount of SNCs injected (Figure S4). This approach for epitaxial growth does not require precise control over the introduction of shell components (injection rate), as often needed with the molecular precursor injection and growth.[1d,e] In molecular precursor mediated epitaxy, to eliminate homogeneous nucleation of the shell precursors and to maintain the narrow temperature window for the precursor decomposition imposes a highly controlled addition step (using a mechanical pump). These variables will lead to difficulties in generating reproducible and tunable epitaxial layer growth.[2a]

To gain insights into the dissolution/growth process, we first studied the growth of core NCs. The solution growth of β-$NaYF_4$ NCs is known to grow in a monomer depleted regime, where the kinetic product (α-$NaYF_4$) formed at lower temperature dissolves at elevated temperature to nucleate into the thermodynamic phase, followed by interparticle ripening to yield uniform β-$NaYF_4$ NCs.[7,9] We confirmed that this is also the case in our system (Figure S5). The yields of the inorganic NC growth carried out for different reaction times (30 min and 1 h) were almost the same at >80%, confirming the monomer depleted interparticle ripening-mediated growth (Figure S6). The growth rate of a particle with size r in this diffusion controlled regime is given by the following eq (1)

$$dr/dt = K(1/r + 1/\delta)(1/r^* - 1/r) \quad (1)$$

where, K is constant proportional to the diffusion constant of the monomer, and δ is the thickness of the diffusion layer.[10] NCs smaller than the critical radius (r^*) dissolve while NCs larger than the critical radius grow at their expense. The critical radius in an ensemble of NCs is the average size number of the ensemble,[11] which increases as the smaller particles are depleted by dissolution/deposition on the larger NCs. When the core NCs focus into a unimodal size distribution, the critical radius (r^*) is about the same as the average size. Thus, deliberately defocusing the ensemble by introducing small SNCs (α-$NaYF_4$) shifts the critical radius to a smaller size. Under this condition, the SNCs rapidly dissolve as they are smaller than the critical radius, and deposit on the larger core NCs, that is, the ensemble refocuses to a narrow unimodal size distribution (σ<5%). Remarkably, the core NCs (Figure 1A) after ripening (Figure 1C) had increased by 70% in volume in just 10 min confirming the rapid dissolution/growth process.

The defocusing and self-focusing cycle can be repeated multiple times to generate layer-by-layer shell growth. TEM images shown in Figure 2A–E and Figures S7–S9 demonstrate the easy control offered by this method in shell thickness tuning, which was achieved by four successive SNC injection (0.2 mmol) and ripening cycles. Varying the quantity of SNCs injected (0.25 mmol) resulted in increased layer thickness in each cycle (Figure S10). The successive growth of epitaxial shells with each cycle is confirmed by the elemental analysis (ICP-MS) of NC dispersions containing the same number of NCs (see SI for details). Figure 2F clearly shows the increase in Y^{3+} while the optically active ions (Yb^{3+} and Er^{3+}) remain the same. The increase in the amount of Y^{3+} after four cycles correlates excellently to the total amount of SNCs injected (see Table S2 for details), confirming the mass balance throughout the ripening cycle. The consistent increase in upconversion emission intensity of both green and red emissions with increasing layer thickness (Figure 2G) with the optically active ion concentration (Yb^{3+} and Er^{3+}) remaining constant further confirms the epitaxial shell growth. Considering the distance dependent Förster mechanism ($1/r^6$) in solvent quenching, the spatial screening of the luminescent core from the solvent environment with each additional layer leads to luminescence enhancement (Figure S11 shows relative increase in

dx.doi.org/10.1021/ja302717u | J. Am. Chem. Soc. 2012, 134, 11068–11071

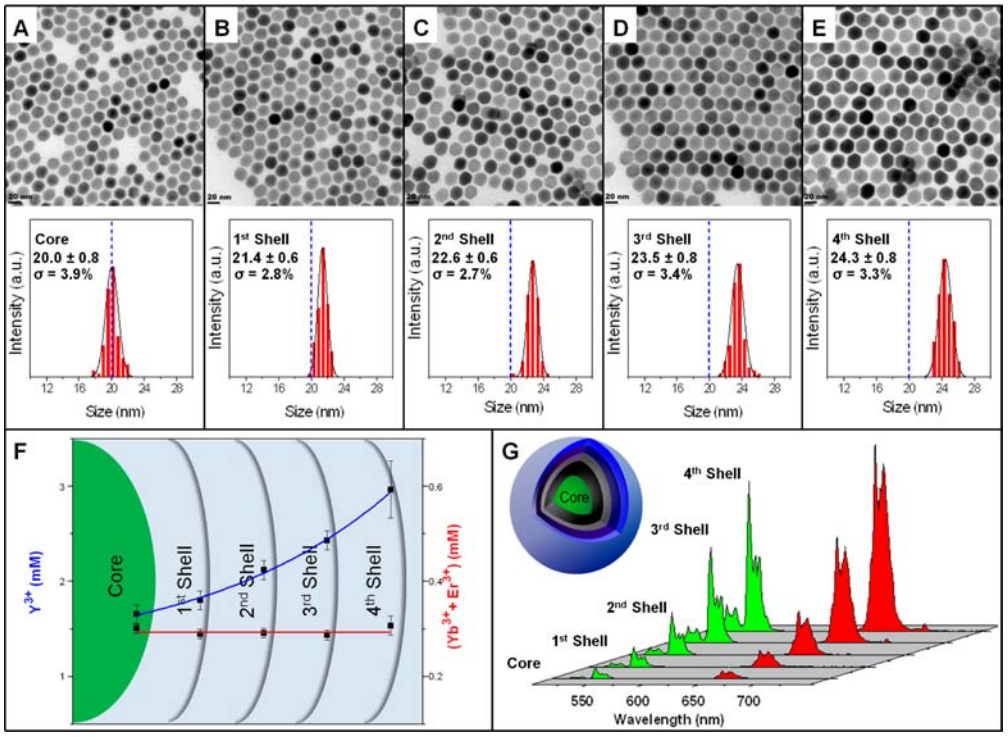

Figure 2. (A–E) TEM images and size distribution of $NaYF_4$:Yb^{3+}/Er^{3+} (15/2%) core NCs (t = 0), $NaYF_4$:Yb^{3+}/Er^{3+} (15/2%) core/$NaYF_4$ shell NCs after successive layer-by-layer epitaxial growth at t = 5, 10, 15, and 20 min, respectively; (F) ICP-MS elemental analysis of the core and core–shell NCs with same number concentration of NCs; (G) upconversion emission spectra of the hexane dispersions of core and core–shell NCs with same number concentration of NCs under 980 nm excitation.

intensities). The size increase from the TEM analysis, alongside the ICP-MS and upconversion emission profiles unequivocally demonstrate the ability to generate core–shell NCs with tunable shells through a layer-by-layer growth by deliberate defocusing of the system and self-focusing by ripening in multiple cycles.

This protocol is versatile and can easily be extended to obtain core–shell NCs of different composition and also to orient spatially dopant ions and layers with variable compositions. A thin layer of $NaGdF_4$ as shell is ideal for integrating magnetic resonance imaging (MRI) and upconversion properties into a single NC, as only the surface gadolinium ions are known to affect the relaxation of water protons.[12] $NaYF_4$/$NaGdF_4$ core–shell NCs could be obtained by injection of hexagonal β-$NaGdF_4$ (5 nm) SNCs into a solution of core β-$NaYF_4$ NCs, and ripening. The size increase of the NCs after ripening (Figure 3A,B and Figure S12) and the absence of the SNCs demonstrate the ability to deposit epitaxial layers of choice by ripening, and that the SNCs of any composition/crystal phase (α /β) can be utilized in the process. The difference in chemical composition of the core (Y^{3+}) and shell (Gd^{3+}) allowed for 2D-elemental mapping by electron energy loss spectroscopy (EELS)[13] to confirm the dissolution and deposition of $NaGdF_4$ on the $NaYF_4$ core NCs (Figure 3C,D and Figure S12). While the core–shell NCs are highly uniform and monodisperse in size (Figure S13A,B), the distribution of the gadolinium ions (Figure 3C,D and Figure S13) as observed from the EELS mapping suggests that some crystal planes may grow at different rates,[13] or might have been etched during plasma cleaning (see experimental details in SI). The fact that we can deliberately control the epitaxial growth utilizing this self-focusing process should allow for further mechanistic

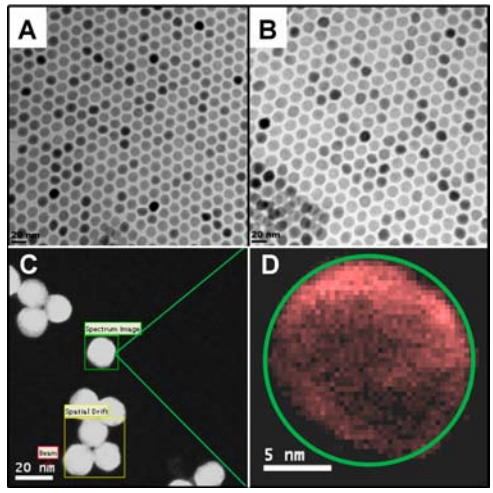

Figure 3. TEM images of (A) $NaYF_4$ core NCs; (B) $NaYF_4$ core/$NaGdF_4$ shell NCs; (C and D) EELS 2D-mapping of gadolinium confirming the deposition of $NaGdF_4$ shell.

investigation of the shell growth, and results pertaining to such study will be the subject of a future publication.

As a proof-of-principle, dual-mode emitting NCs were obtained using this protocol either by spatially orienting different dopant ions in the same matrix (Figure S14) or by simultaneously varying both the matrix and dopant ions (Figure S16). This further demonstrates the utility of this self-focusing by ripening approach to orient easily dopant ions and layers of variable compositions without any deleterious cross-relaxation as observed with codoped NCs of the same dopant concentrations (Figures S15 and S17). Recent confirmation

dx.doi.org/10.1021/ja302717u | J. Am. Chem. Soc. 2012, 134, 11068–11071

of core−shell structure at subnanometer level using cryo-TEM analysis for the same class of materials has indeed shown a sharp interface between the core and shell.[14] This confirms that the shell composition is not significantly altered during growth by intermixing of layers driven by exchange of materials[15] along the core−shell interface. This self-focusing approach to generate dual-mode emitting core−shell NCs can be extended for relatively smaller sized upconverting $NaGdF_4$ NCs as shown in Figures S18 and S19.

In summary, we have presented a versatile epitaxial growth technique based on a common physical phenomenon of ripening in colloids to grow shells tunable both in thickness and composition. The protocol is flexible and allows to deposit easily multiple layers by successive defocusing and self-focusing cycle without the need for multistep process. Moreover, the ripening-mediated epitaxial growth facilitates NCs with narrow size distribution, as the NCs spontaneously self-focus by dissolution of the energetically less favored SNCs in the ensemble. This approach only requires the SNCs to be smaller than the core NCs, and does not necessitate any stringent control over the introduction of shell components as needed for precursor injection and shell growth. This added advantage should allow for easy automation and scaled-up synthesis of high quality core−shell NCs as their scope widens in various applications. Finally, as this approach relies on a fundamental colloidal property, it is pertinent for NCs in general to overcome the limitations of conventional shell growth techniques.

■ ASSOCIATED CONTENT

Supporting Information

Experimental details for NC synthesis, related characterization, and supplementary results and discussion; complete ref 1e. This material is available free of charge via the Internet at http://pubs.acs.org.

■ AUTHOR INFORMATION

Corresponding Author

fvv@uvic.ca

Notes

The authors declare no competing financial interest.

■ ACKNOWLEDGMENTS

We thank the Natural Science and Engineering Research Council (NSERC), the Canada Foundation for Innovation (CFI), and the British Columbia Knowledge Development Fund (BCKDF) for funding. Dr. Jody Spence (UVIC) acknowledged for ICP-MS analysis. EELS mapping was performed at the Canadian Centre for Electron Microscopy, supported by NSERC & other government agencies.

■ REFERENCES

(1) (a) Wang, F.; Wang, J. A.; Liu, X. G. *Angew. Chem., Int. Ed.* **2010**, *49*, 7456. (b) Boyer, J. C.; van Veggel, F. C. J. M. *Nanoscale* **2010**, *2*, 1417. (c) Yi, G. S.; Chow, G. M. *Chem. Mater.* **2007**, *19*, 341. (d) Vetrone, F.; Naccache, R.; Mahalingam, V.; Morgan, C. G.; Capobianco, J. A. *Adv. Funct. Mater.* **2009**, *19*, 2924. (e) Il Park, Y.; et al. *Adv. Mater.* **2009**, *21*, 4467. (f) Qian, H. S.; Zhang, Y. *Langmuir* **2008**, *24*, 12123.

(2) (a) Haase, M.; Schafer, H. *Angew. Chem., Int. Ed.* **2011**, *50*, 5808. (b) Wang, F.; Liu, X. G. *Chem. Soc. Rev.* **2009**, *38*, 976. (c) Wang, G. F.; Peng, Q.; Li, Y. D. *Acc. Chem. Res.* **2011**, *44*, 322. (d) Zhou, J.; Liu, Z.; Li, F. Y. *Chem. Soc. Rev.* **2012**, *41*, 1323.

(3) (a) Carling, C. J.; Nourmohammadian, F.; Boyer, J. C.; Branda, N. R. *Angew. Chem., Int. Ed.* **2010**, *49*, 3782. (b) Wang, M.; Hou, W.; Mi, C. C.; Wang, W. X.; Xu, Z. R.; Teng, H. H.; Mao, C. B.; Xu, S. K. *Anal. Chem.* **2009**, *81*, 8783. (c) Wu, W.; Yao, L. M.; Yang, T. S.; Yin, R. Y.; Li, F. Y.; Yu, Y. L. *J. Am. Chem. Soc.* **2011**, *133*, 15810. (d) Wang, F.; Deng, R.; Wang, J.; Wang, Q.; Han, Y.; Zhu, H.; Chen, X.; Liu, X. *Nat. Mater.* **2011**, *10*, 968. (e) Schietinger, S.; Aichele, T.; Wang, H. Q.; Nann, T.; Benson, O. *Nano Lett.* **2010**, *10*, 134.

(4) Wang, F.; Han, Y.; Lim, C. S.; Lu, Y. H.; Wang, J.; Xu, J.; Chen, H. Y.; Zhang, C.; Hong, M. H.; Liu, X. G. *Nature* **2010**, *463*, 1061.

(5) Talapin, D. V.; Rogach, A. L.; Haase, M.; Weller, H. *J. Phys. Chem. B* **2001**, *105*, 12278.

(6) (a) Chen, Y.; Johnson, E.; Peng, X. *J. Am. Chem. Soc.* **2007**, *129*, 10937. (b) Talapin, D. V.; Lee, J.-S.; Kovalenko, M. V.; Shevchenko, E. V. *Chem. Rev.* **2010**, *110*, 389. (c) Thessing, J.; Qian, J.; Chen, H.; Pradhan, N.; Peng, X. *J. Am. Chem. Soc.* **2007**, *129*, 2736. (d) Kwon, S. G.; Piao, Y.; Park, J.; Angappane, S.; Jo, Y.; Hwang, N.-M.; Park, J.-G.; Hyeon, T. *J. Am. Chem. Soc.* **2007**, *129*, 12571.

(7) Mai, H. X.; Zhang, Y. W.; Sun, L. D.; Yan, C. R. *J. Phys. Chem. C* **2007**, *111*, 13730.

(8) Li, Z. Q.; Zhang, Y.; Jiang, S. *Adv. Mater.* **2008**, *20*, 4765.

(9) (a) Yi, G. S.; Chow, G. M. *Adv. Funct. Mater.* **2006**, *16*, 2324. (b) Mai, H. X.; Zhang, Y. W.; Si, R.; Yan, Z. G.; Sun, L. D.; You, L. P.; Yan, C. H. *J. Am. Chem. Soc.* **2006**, *128*, 6426.

(10) Peng, X. G.; Wickham, J.; Alivisatos, A. P. *J. Am. Chem. Soc.* **1998**, *120*, 5343.

(11) Finsy, R. *Langmuir* **2004**, *20*, 2975.

(12) (a) Chen, F.; Bu, W. B.; Zhang, S. J.; Liu, X. H.; Liu, J. N.; Xing, H. Y.; Xiao, Q. F.; Zhou, L. P.; Peng, W. J.; Wang, L. Z.; Shi, J. L. *Adv. Funct. Mater.* **2011**, *21*, 4285. (b) Johnson, N. J. J.; Oakden, W.; Stanisz, G. J.; Prosser, R. S.; van Veggel, F. C. J. M. *Chem. Mater.* **2011**, *23*, 3714.

(13) Abel, K. A.; Boyer, J.-C.; Andrei, C. M.; van Veggel, F. C. J. M. *J. Phys. Chem. Lett* **2011**, 185.

(14) Zhang, F.; Che, R.; Li, X.; Yao, C.; Yang, J.; Shen, D.; Hu, P.; Li, W.; Zhao, D. *Nano Lett.* **2012**, *12*, 2852.

(15) Dong, C.; Korinek, A.; Blasiak, B.; Tomanek, B.; van Veggel, F. C. J. M. *Chem. Mater.* **2012**, *24*, 1297.